



Effect of powder grinding and sintering temperature on structure and properties of $\text{Ba}_{0.8}\text{Ca}_{0.2}\text{TiO}_3$ ceramics

Magdalena Gromada^{✉*}

Institute of Power Engineering – National Research Institute, 01-330 Warsaw, Mory 8, Ceramic Division CEREL, Techniczna 1, 36-040 Boguchwała, Poland

Received 16 November 2024; Received in revised form 8 March 2025; Accepted 16 March 2025

Abstract

Lead-free barium-calcium titanate (BCT) ceramics were prepared via the solid-state method and sintering at different temperatures. The influence of BCT powder grinding on particle morphology, porosity and particle size distribution was investigated. The effect of sintering temperature on microstructure and mechanical properties of the BCT ceramics was also analysed. BCT material sintering optimization was connected with providing high density and ensuring the smallest grain sizes. The sintered BCT material with the optimized parameters had apparent density of 5.49 g/cm^3 and homogeneous, densely packed microstructure consisting of grains ranging from 1 to $5 \mu\text{m}$, as well as bending strength reaching 147 MPa, hardness of the level of 4.83 GPa and fracture toughness equal to $1.86 \text{ MPa}\cdot\text{m}^{0.5}$. The developed BCT material in this paper possesses favourable functional properties that allow its use in multilayer actuators.

Keywords: barium-calcium titanate, perovskite, structure, mechanical properties

I. Introduction

Lead-based ferroelectrics (PZT and PT) are substantially employed as piezoelectric sensors, actuators and transducers due to their superior piezoelectric properties [1–3]. At the same time, evaporation of toxic PbO in the sintering process pollutes the environment and changes product composition, forming ceramics with unstable electrical qualities.

Presently, intensive work has led to the development of the lead-free piezoelectric materials (BCT, BZT, NBT, KBT) for applications in sensors, actuators and energy storage devices. These studies are highly important because most of the used piezoelectrics contain harmful lead and this element should be eliminated from the European market in the near future [4–8].

Barium titanate-based perovskite materials, which exhibit ferroelectric and piezoelectric properties, are very attractive for use in the fields of microelectronics and medicine. Among many available piezoelectric materials, barium-calcium titanate $\text{Ba}_{0.8}\text{Ca}_{0.2}\text{TiO}_3$ (BCT) has been widely studied because its properties are similar to those of lead-containing PZT materials [9,10].

The synthesis and characterization of barium-calcium titanate have been the subject of several publications, which show that the properties of powders and sintered materials depend on the synthesis procedure and sintering conditions. Usually, very complicated and laborious methods were used for producing this material: modified Pechini method, sol-gel method, hydrothermal method and co-precipitation [9,11–13]. Several research papers are devoted to piezoelectric materials synthesised by mechanical activation and solid state reaction. These methods can be easily upscaled, enable strict stoichiometry control and bring economic benefit [6,10,14,15].

The use of piezoelectric materials for multilayer actuators requires a high density of sintered material, a high dielectric constant and a low dielectric loss factor. The electrical properties of ceramics are closely related to their microstructure. Thus, the most advantageous materials are characterised by small grains of a few micrometres in size, which are well separated by intergranular boundaries without pores [16,17]. Researchers have tried to optimize the microstructure of PZT-type materials by intensifying the mechanical activation processing of powders and reducing sintering temperature due to the lower calcination temperature of the internal elec-

*Corresponding authors: tel: +48 504 745 364,
e-mail: magdalena.gromada@cerel.pl

trodes in multilayer actuators, but this can lead to the deterioration of other properties of the materials [18–21].

Presently, many articles are dedicated to the synthesis methods and determination of the properties of BaTiO₃ material or Ca-doped barium titanate. Feliksiak *et al.* [22] underlined the significant impact of sintering temperature on the microstructure and dielectric properties of Ba_{0.75}Ca_{0.25}TiO₃ and structural and functional properties of this material. Khedhri *et al.* [23] analysed the structural, spectroscopic and optical properties of Ba_{1-x}Ca_xTiO₃ ceramics with $x < 0.2$ prepared by sol-gel method at low temperature. Borkar *et al.* [24] investigated the influence of calcium substitution on structural, dielectric, ferroelectric, piezoelectric and energy storage properties of BaTiO₃ material. Basumatary *et al.* [25] studied the structural, microstructural, dielectric, optical, ferroelectric and magnetic properties of cobalt doped barium calcium titanate (Ba_{0.80}Ca_{0.20}Ti_{1-x}Co_xO₃ with $x = 0, 0.005, 0.010, 0.015$ and 0.020) material. Dhahri *et al.* [26] synthesised Ba_{0.95}Ca_{0.05}Ti_{0.97}Y_{0.04}O₃ powder by solid state method and investigated its physical properties.

The aim of this work is to investigate the effect of mechanical activation of Ba_{0.8}Ca_{0.2}TiO₃ (BCT) powder on particle and pore size distribution, morphology and porosity. In addition, the influence of milling time and sintering temperature on the microstructure and other functional parameters was also analysed.

II. Experimental

2.1. Sample preparation

Barium-calcium titanate with a Ba_{0.8}Ca_{0.2}TiO₃ (BCT) composition was synthesized via the solid-state method with the use of titanium oxide (TiO₂ 99%, Kronos), barium carbonate (BaCO₃ 99.5%, Chempur) and calcium carbonate (CaCO₃ 99%, Chempur). The set of raw materials was mixed in a polyethylene beaker with isopropyl alcohol at a ratio of 1:1 and then poured into an attritor with the working chamber $\varnothing 135 \times 180$ mm. The components were mechanically activated for 2 h at 280 rpm with zirconia grinding balls with a diameter of 3 mm and a weight of 4.5 kg. The obtained suspension was dried at 70 °C and the dried powder was calcined at 1100 °C for 4 h with the heating rate of 100 °C/h (named the as-prepared BCT powder). The selected temperature was determined experimentally taking into account phase compositions of the samples calcined at 900, 1000 and 1100 °C. The four hours dwell time at the maximal temperature ensured sufficient time for temperature penetration inside the sample and complete synthesis.

Additional milling of the BCT powder was performed to decrease particle size and carried out in an attritor at 560 rpm with zirconia grinding balls with a diameter of 3 mm and a weight of 4.5 kg. Three different milling times were used: 30 min, 2 h and 4 h and the corresponding samples (named the milled BCT powder) were designated as BCT-1, BCT-2 and BCT-3, respec-

tively. In the next step, for the pellet fabrication, it was necessary to make granulates to improve the pressing properties. Thus, the BCT-1, BCT-2 and BCT-3 powders were dispersed in deionized water at a ratio of 1:1 together with the following additives: 0.2% Dispex, 0.2% oil emulsion and 1% polyvinyl alcohol. Granulates were formed in a spray dryer (Niro atomizer) with a 372A peristaltic pump (ELPIN-PLUS s.c.). Air atomization was used through an air nozzle, and the following drying conditions were applied: inlet temperature of 220 °C, outlet temperature of 80 °C and spray pressure of 40 mm in the water column. After that, a pressing mould with an internal diameter of $\varnothing 11.5$ mm was filled with 1.5 g of the BCT-1, BCT-2 and BCT-3 granulates and the corresponding pellets were obtained by uniaxial pressing at 2 MPa and then isostatic pressing at 150 MPa. The rectangular samples were shaped via a truncated circular mould on a TPA 15/4 press (Dorst) under the pressure of 10 MPa and then isostatically pressed at 150 MPa, as in the case of the pellets.

2.2. Characterization

Phase composition analysis of the BCT powder was performed on a Miniflex II X-ray diffractometer (Rigaku). The measurements were carried out via CuK α radiation in an angular range of $2\theta = 20^\circ - 80^\circ$ with a step of 0.02° and a counting time of 3 s. The phase composition was determined using the Powder Diffraction File (PDF) database developed by ICDD (The International Centre for Diffraction Data). The phase components were identified by matching the profile of the obtained diffraction pattern - the calculated distances between the dhkl planes for individual reflections and their intensities to the data contained in the PDF database. The particle size distribution of the prepared powders was determined via laser diffraction on a Mastersizer 2000 granulometer (Malvern). The morphology of the powders and microstructure of the sintered ceramics were studied using a Zeiss Crossbeam 350 SEM. ImageJ Fiji software was used to find the particle size from SEM images. The pore size distribution and pore volume of the BCT powder was determined with an AUTOPORE 4 9500 (Micromeritics) via mercury porosimetry method.

The dilatometric analysis of the BCT-1, BCT-2 and BCT-3 green bodies, not presented here, was used to select appropriate thermal treatments for sintering, as following: the maximal sintering temperatures were 1250, 1300 and 1350 °C, the heating and cooling rates were 100 °C/h and the dwell time was 4 h.

Apparent density and open porosity of the prepared samples were determined via Archimedes' principle and the boiling method to saturate the samples with water. The hardness and fracture toughness (K_{IC}) were measured using a 430/450SVD Vickers hardness tester. The samples were first embedded in acrylic resin and then ground on #500 and #1200 diamond discs. The final processing was performed using a polishing cloth with a diamond suspension of grain size equal to 3 and 1 μm .

The bending strength was determined by the three-point method on sintered not polished beams with flattened circular cross-section via a ZDM-5 testing machine.

III. Results and discussion

3.1. As-prepared BCT powder

Figure 1 shows X-ray diffraction pattern of the as-prepared BCT powder after mechanical activation and calcination at 1100 °C, which indicates the presence of an ideal perovskite structure of the BCT material. The spectrum is free of noise and the peaks are perfectly matched to those of the standard. The quantitative analysis of the powder phase composition revealed the presence of the $\text{Ba}_{0.8}\text{Ca}_{0.2}\text{TiO}_3$ phase with a tetragonal structure. However, a small amount less than 3% of $\text{Ba}_{0.128}\text{Ca}_{0.872}\text{TiO}_3$ phase with a cubic structure is also visible in XRD spectrum and one minor peak originating from CaO oxide.

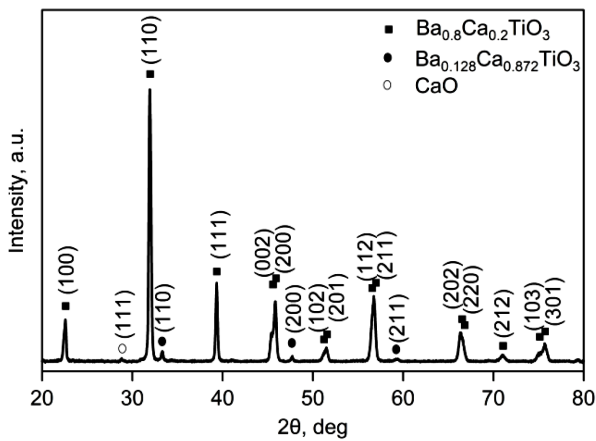


Figure 1. XRD spectrum of BCT powder calcined at 1100 °C

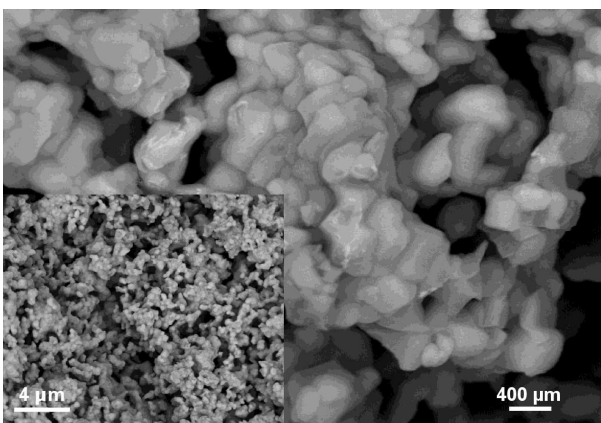


Figure 2. SEM image of BCT powder

SEM image the as-prepared BCT powder calcined at 1100 °C (Fig. 2) confirmed the presence of large, porous particles of up to 50 μm in size, composed of smaller, tightly bonded grains of up to 0.3 μm.

Figure 3 presents the particle size distribution of the BCT powder after mechanical activation and calcination

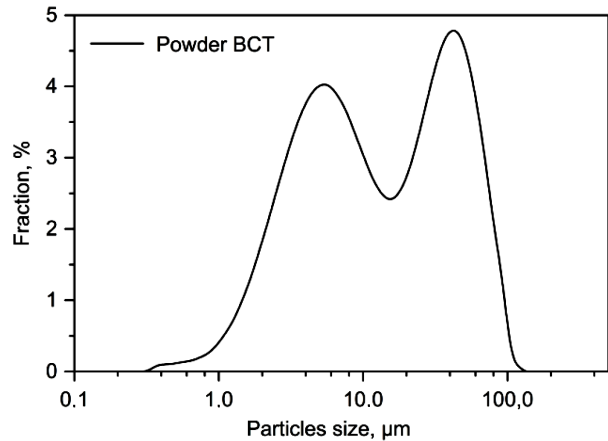


Figure 3. Particle size distribution of BCT powder after calcination at 1100 °C

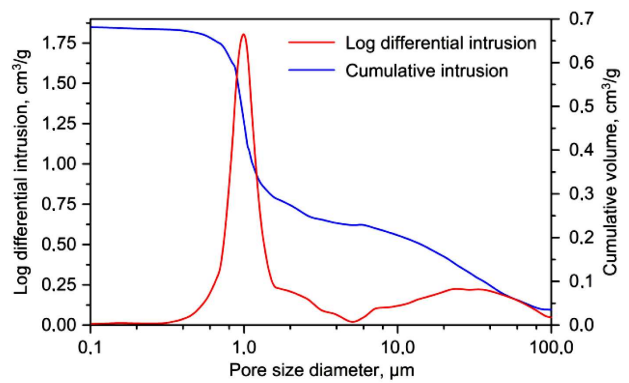


Figure 4. Differential and cumulative curves of the pore size distribution of the BCT powder

at 1100 °C. The distribution of particle sizes is very wide and ranges from 0.3 to 120 μm with the calculated average particle size of 11.6 μm. The bimodal distribution of the BCT powder indicates that the grains are agglomerated, which is confirmed by BCT powder morphology result presented in Fig. 2.

Figure 4 presents the differential and cumulative curves of the pore size distribution of the as-prepared BCT powder. The peak abscissa of the differential curve indicates the average pore size, which is 1.21 μm. The cumulative pore volume was 684 mm³/g, the apparent density reached 5.06 g/cm³ and the porosity was 77.6%. Therefore, the BCT powder is characterized by porous particles with larger pore sizes, which is consistent with the SEM images of the powder morphology shown in Fig. 2.

3.2. Milled BCT powders

The particle size distributions of the BCT-1, BCT-2 and BCT-3 powders are shown in Fig. 5 and indicate that with the increase of the milling time curves shifted more towards smaller particles than for the as-prepared BCT powder (Fig. 2). The average particle size decreased to 2.39, 1.44 and 1.22 μm for the BCT-1, BCT-2 and BCT-3 powders, respectively. Furthermore, all distributions are narrower and almost unimodal with particle sizes

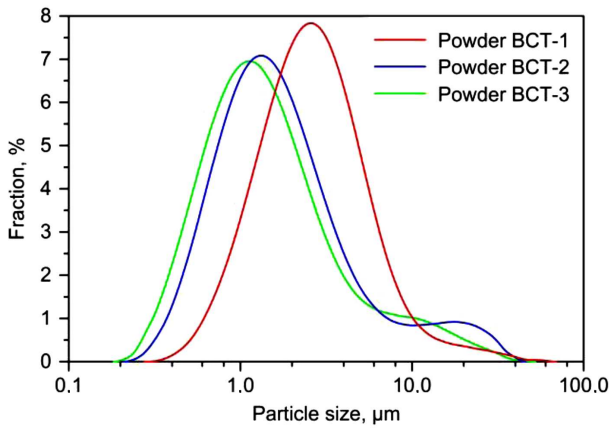


Figure 5. Particle size distributions of milled powders (BCT-1, BCT-2 and BCT-3)

varying from 0.2 to 40 μm and with a distinct shoulder in the range of larger particles, which indicates that the tendency to form agglomerates still exists.

SEM images of the milled powders (Fig. 6) clearly indicate that this process disrupted the connected powder grains, thus the average pore size and porosity were reduced and the cumulative pore volume was increased. Thus, for the BCT-1 powder milled for 30 min (Fig. 6a), clusters of tightly connected particles are visible, but large particles have already been disrupted. The average grain size of the BCT-1 powder did not change significantly and it is equal to 0.3 μm, but much smaller grains are also visible.

In the micrograph of the BCT-2 powder milled for 2 h (Fig. 6b) greater powder packing, resulting from better disruption of the connected grains, is clearly visible. The average grain size of the BCT-2 powder decreased to 0.2 μm and there were also many smaller grains. Even greater fragmentation and, consequently, denser packing characterize the BCT-3 powder (Fig. 6c). Most of the grains are up to 0.2 μm in size, but many smaller grains are also visible. The results of powder morphology are in accordance with the particle size distribution presented in Fig. 5, porosity shown in Fig. 7 and data in Table 1.

Differential pore size distributions and cumulative pore size distributions of the BCT-1, BCT-2 and BCT-3 powders are shown in Figs. 7a and 7b respectively. The average pore sizes of the BCT-1, BCT-2 and BCT-3 powders are 0.71, 0.86 and 0.62 μm, respectively. These values take into account an additional peak of the differential curve in the area of pore sizes ranging from 10 to 100 μm (Fig. 7a). On the other hand, in the region of pore sizes occurring in powder particles, with increasing of the milling time, the average pore size decreases. Moreover, the increase of milling time caused an increase in the cumulative pore volume and, to a small extent, porosity and a decrease in the apparent density of the BCT powders. Thus, the increased milling time of the powders resulted in the formation of particles with smaller but more numerous pores, which is consistent with the SEM images of the powder morphology presented in Fig. 6. This observation is confirmed by

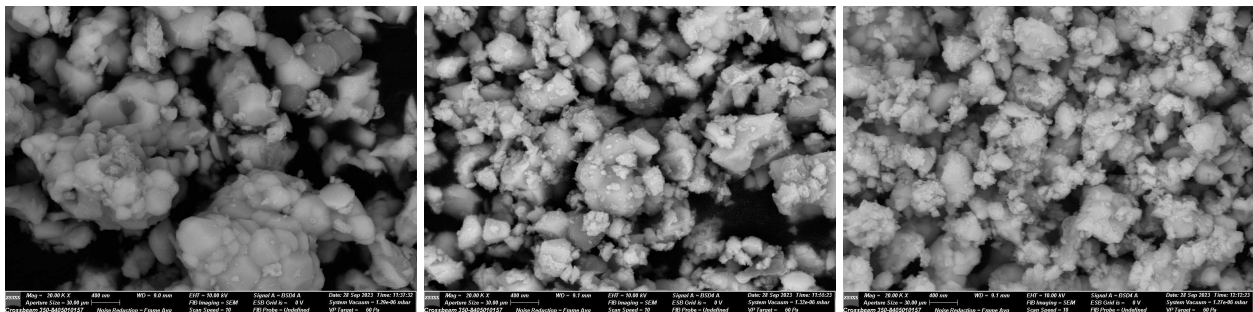


Figure 6. SEM images of milled powders: a) BCT-1, b) BCT-2 and c) BCT-3

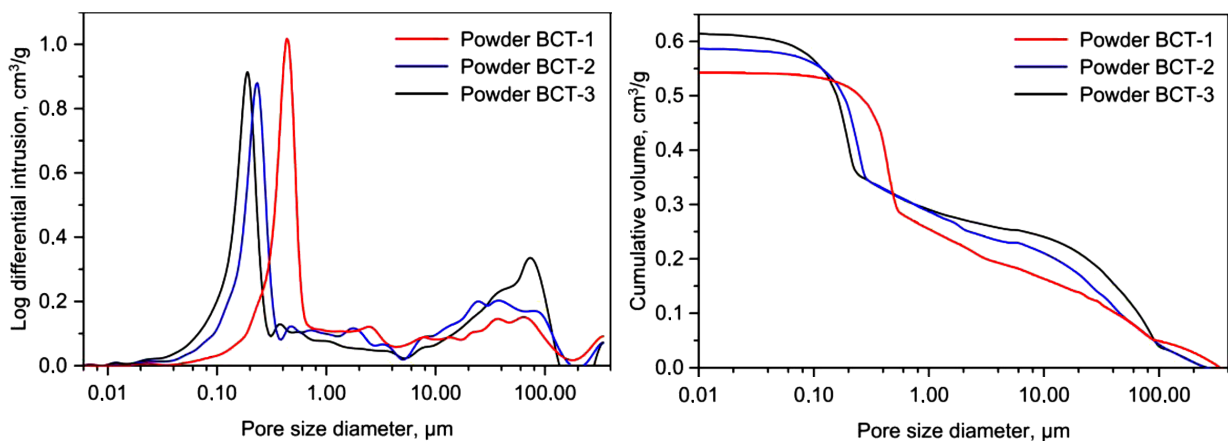


Figure 7. Differential (a) and cumulative (b) pore size distribution curves for the BCT-1, BCT-2 and BCT-3 powders

Table 1. Porosity parameters of the milled BCT-1, BCT-2 and BCT-3 powders

Powder	Average pore diameter [μm]	Cumulative pore volume [mm^3/g]	Apparent density [g/cm^3]	Porosity [%]
BCT-1	0.71	542.5	5.04	73.22
BCT-2	0.86	586.5	4.80	73.82
BCT-3	0.62	614.6	4.75	74.51

the results of the characteristic quantities describing the porosity of the BCT powders, which are summarized in Table 1.

3.3. Sintered samples

SEM surface analyses of the sintered BCT pellets are shown in Figs. 8–10. The microstructure of the BCT-1 pellet sintered at 1250 °C (Fig. 8a) is homogeneous, densely packed and consists of small, angular grains ranging from 1 to 5 μm . However, small pores between the grain boundaries are clearly visible. The SEM image of the BCT-2 pellet sintered at 1250 °C (Fig. 8b) reveals bimodal grain size distribution, fine ones ranging from 1 to 2 μm together with a significant number of large grains quite evenly distributed over the entire surface with a size of up to 20 μm . The microstructure of the BCT-3 pellet sintered at 1250 °C (Fig. 8c) consists of fine grains with sizes reaching 1–2 μm . Moreover, the surface of the ceramics is very homogeneous, but some pores between the grains can be seen.

Increasing the maximum sintering temperature by 50 °C resulted in a significant increase in the grain size, especially for the BCT-1 and BCT-2 materials sintered at 1300 °C. In the case of the BCT-1 pellets sintered at 1300 °C (Fig. 9a), fine grains of 2–5 μm and larger grains of up to 20 μm can be distinguished on the surface. Together with larger grains, fine grains constitute a well-packed structure. The surface of the BCT-2 pellet

sintered at 1300 °C (Fig. 9b) is characterized by an even greater number of large grains reaching up to 30 μm , and only in their corners there are a few single small grains. The effect of grain growth is also visible in the case of the BCT-3 ceramics sintered at 1300 °C (Fig. 9c). Grains of up to 2 μm predominate, but there are also single grains of up to 5–6 μm .

Another increase in the maximum sintering temperature of 50 °C caused additional structure coarsening but the grain size distribution became more uniform (Fig. 10). In the case of the BCT-1 pellet sintered at 1350 °C (Fig. 10a), the most of grains are with sizes of up to 8–10 μm and few grains exceeding 15 μm . The SEM micrographs of the BCT-2 pellet sintered at 1350 °C (Fig. 10b) show grains with sizes of 15–20 μm together with some smaller grains situated only in the corners. On the other hand, the surface microstructure of the BCT-3 pellet sintered at 1350 °C (Fig. 10c) gives impression of being clearly burnt. The grain boundaries are surrounded by melted grains, the grain surface is uneven and non-uniform, and the grain sizes range from 2–30 μm . For this reason, the porosity is not visible and their bending strength is very high (Table 2). However, a material with this type of microstructure cannot be used for multilayer actuators.

Properties of the prepared ceramics sintered at temperatures ranging from 1250 to 1350 °C are given in Table 2. For the ceramics sintered at 1250 °C the appar-

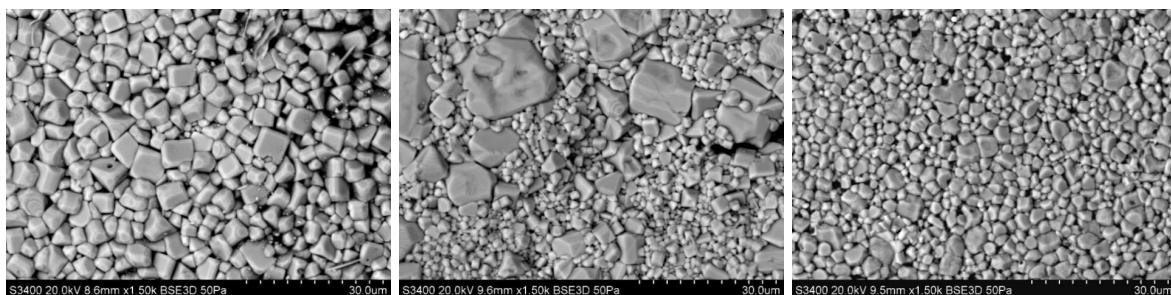


Figure 8. SEM micrographs of: a) BCT-1, b) BCT-2 and c) BCT-3 material sintered at 1250 °C

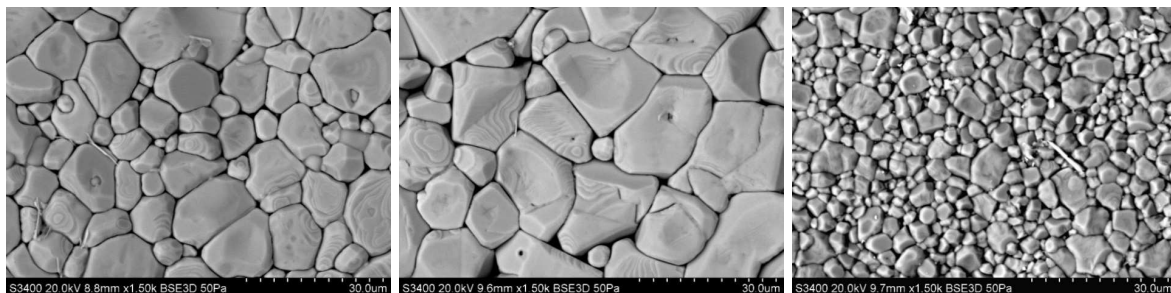


Figure 9. SEM micrographs of: a) BCT-1, b) BCT-2 and c) BCT-3 material sintered at 1300 °C

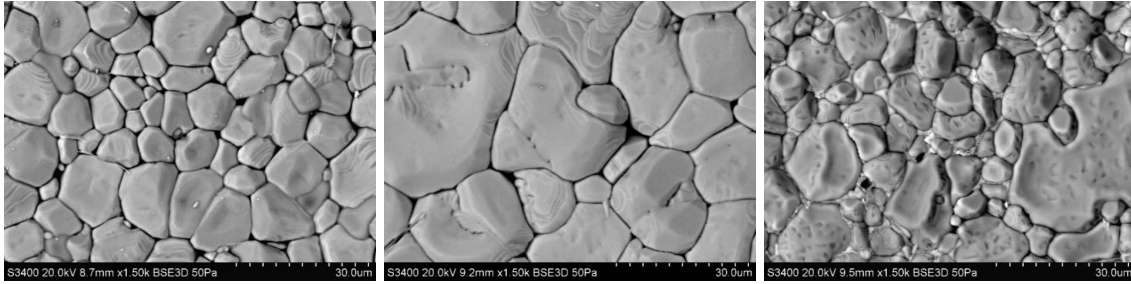


Figure 10. SEM micrographs of: a) BCT-1, b) BCT-2 and c) BCT-3 material sintered at 1350 °C

Table 2. Properties of BCT materials sintered at 1250, 1300 and 1350 °C

Material	ρ_A [g/cm ³]	P_O [%]	H_V [GPa]	K_{IC} [MPa·m ^{0.5}]	σ [MPa]
BCT-1 1250 °C	5.49	0.07	4.83	1.86	147
BCT-2 1250 °C	5.42	0.10	4.51	2.01	146
BCT-3 1250 °C	5.22	3.88	4.32	1.93	109
BCT-1 1300 °C	5.45	0.60	4.50	1.84	141
BCT-2 1300 °C	5.41	1.32	4.28	1.92	145
BCT-3 1300 °C	5.42	0.26	5.41	1.75	141
BCT-1 1350 °C	5.43	0.86	4.70	1.72	144
BCT-2 1350 °C	5.40	1.48	3.85	1.66	136
BCT-3 1350 °C	5.52	0.05	4.34	1.86	142

ent density decreases and open porosity increases with increasing milling time. The same relationship for the hardness and bending strength can be noticed. Along with increasing milling time of the powders, the hardness and bending strength of the sintered ceramics decreased. What is interesting, such trend is not visible for the fracture toughness. The highest fracture toughness is noticed for the material BCT-2 originated from powder milled for 2 h.

In the case of the ceramics sintered at 1300 and 1350 °C, the apparent density and hardness decrease for the BCT-2 and increase for the BCT-3 sample. The opposite connection occurs for open porosity of these materials. Quite different tendency occurs in the case of the fracture toughness and bending strength of the materials sintered at 1300 and 1350 °C. For the materials sintered at 1300 °C, fracture toughness and strength increase for the sample obtained from the powder milled for 2 h and decrease for the sample BCT-3 obtained from the powder milled for 4 h. However, for the materials sintered at 1350 °C, fracture toughness and bending strength decrease for the sample BCT-2 and then increase for the sample BCT-3.

In the case of the material BCT-1 obtained from the powder milled for 30 min, the apparent density and fracture toughness decrease with sintering temperature. Hardness and bending strength decrease at 1300 °C and then increase at 1350 °C, but these parameters did not reach the level as for the material sintered at 1250 °C. For the material BCT-2 apparent density, hardness, fracture toughness and bending strength decrease with the increasing sintering temperature. In the case of the BCT-3 material, the apparent density and bending strength increase with increasing the maximal sintering tempera-

ture. The hardness of the BCT-3 ceramics was increased at 1300 °C, but decreased when sintered at 1350 °C. The opposite tendency was also noticed for the fracture toughness.

The data given in Table 2 shows that the BCT-3 sintered at 1350 °C reveals the highest apparent density equal to 5.52 g/cm³, which is 96% of the theoretical density. Exactly such level of the theoretical density was achieved by Feliksik *et al.* [10]. The highest hardness equal to 5.41 GPa was obtained for the BCT-3 sintered at 1300 °C, which is 22% lower in comparison with results given by Hwang *et al.* [27]. The highest fracture toughness reaching 2.01 MPa·m^{0.5} was obtained for the BCT-2 sintered at 1250 °C. This result is almost two and half time better in comparison with result reported by Hwang *et al.* [27] and 25% better than the one obtained by Chen *et al.* [28]. The highest bending strength equal to 147 MPa was obtained for the BCT-1 sintered at 1250 °C, which is 84% of value obtained by Hwang *et al.* [27] and makes almost three times better result than reported by Chen *et al.* [28].

Taking into account the above presented analysis, the BCT-1 ceramics sintered at 1250 °C has the most advantageous parameters. This material is characterized by almost the highest apparent density, quite high hardness and one of the highest fracture toughness values. In addition, the BCT-1 material sintered at 1250 °C has the highest bending strength among all the materials.

IV. Conclusions

Lead-free Ba_{0.8}Ca_{0.2}TiO₃ (BCT) ceramics were prepared via the solid-state method and sintering at different temperatures. The influence of milling time and

sintering temperature on the structure and mechanical properties was investigated. The BCT ceramics of the most favourable properties originated from the BCT-1 powder, which was milled for 30 min. This powder revealed an average particle size of $2.39\ \mu\text{m}$ characterized by agglomerated particles composed of small grains (up to $0.3\ \mu\text{m}$). The apparent density of the BCT ceramics obtained from BCT-1 powder and sintered at $1250\ ^\circ\text{C}$ is equal to $5.49\ \text{g/cm}^3$. The surface of the BCT material was homogeneous and densely packed and consisted of small, angular grains with a size of 1 to $5\ \mu\text{m}$ and small amount of pores. The BCT-1 ceramics sintered at $1250\ ^\circ\text{C}$ has a high mechanical strength equal to $147\ \text{MPa}$, hardness reaching $4.83\ \text{GPa}$ and fracture toughness of $1.86\ \text{MPa}\cdot\text{m}^{0.5}$.

Acknowledgement: This work was financed by funds for statutory activities No. OC/02/STAT/2023 realized by Institute of Power Engineering – National Research Institute Ceramic Division CEREL.

References

1. C.A. Oliveira, E. Longo, J.A. Varela, M.A. Zaghete, "Synthesis and characterization of lead zirconate titanate (PZT) obtained by two chemical methods", *Ceram. Int.*, **40** [1B] (2014) 1717–1722.
2. A. Nayak, S.K. Patri, B. Behera, "Impact of site modification on the functional properties of PbTiO_3 : A review", *Mater. Sci. Eng. B*, **309** (2024) 117633.
3. S. Kaur, M. Arora, S. Kumar, P.S. Malhi, M. Singh, A. Singh, "Agreement in experimental and theoretically obtained electrocaloric effect in optimized Bi^{3+} doped $\text{PbZr}_{0.52}\text{Ti}_{0.48}\text{O}_3$ material", *J. Adv. Dielect.*, **12** (2022) 2250003.
4. A. Mandal, D. Yadav, S.K. Mittal, U. Jamwal, D. Kaneria, A. Khokhar, M. Jakhar, K.L. Yadav, "Investigation of structural, morphological, dielectric, optical, and ferroelectric-energy storage properties of [(1-x)BCT-(x)BZT] electroceramics", *J. Alloys Compd.*, **995** (2024) 174817.
5. I. Ullah, M. Ur Rehman, A. Manan, M.T. Lanagan, R. Wali Khan, A. Ullah, S. Wali Ullah, M. Uzair, "Structural, dielectric, electrical, and energy storage properties of Mn-doped $\text{Ba}_{0.55}\text{Sr}_{0.45}\text{TiO}_3$ ceramic", *Int. J. Appl. Ceram. Technol.*, **21** [5] (2024) 3413–3421.
6. H.J. Sumona, A.A. Mahmood, M.B. Islam, J.H. Kasem, M.S. Rahman, "Modification of structural, morphological, and dielectric properties of barium calcium titanate ceramics with yttrium addition", *Heliyon*, **10** (2024) e27124.
7. S. Islam, M.R. Molla, N. Khatun, N.I. Tanvir, M. Hakim, Md.S. Islam, "Exploring the effects of zirconium doping on barium titanate ceramics: structural, electrical, and optical properties", *Mater. Adv.*, **6** [4] (2025) 1403–1413.
8. S. Kaur, M. Arora, L. Sharma, S. Kumar, P.S. Malhi, M. Singh, A. Singh, "Hopping mechanism and impedance properties of Mg doped NBT-KBT solid solution near ambient temperature", *ECS J. Solid State Sci. Technol.*, **11** (2022) 103010.
9. L. Kozielski, A. Wilk, M.M. Bućko, J. Banys, "A large piezoelectric strain recorded in BCT ceramics obtained by a modified Pechini method", *Materials*, **13** (2020) 1620.
10. K. Feliksik, L. Kozielski, I. Szafraniak–Wiza, T. Goryczka, M. Adamczyk–Habrajaska, "Dielectric and impedance studies of (Ba,Ca) TiO_3 ceramics obtained from mechanically synthesized powders", *Materials*, **12** (2019) 4036.
11. M.M. Bućko, A. Wilk, J. Lis, A. Toczek, L. Kozielski, "Photoluminescence and electrical properties in Pr-modified $(\text{Ba}_{1-x}\text{Ca}_x)\text{TiO}_3$ multifunctional ceramics", *Process. Appl. Ceram.*, **14** [1] (2020) 77–82.
12. A.E. Souza, R.A. Silva, G.T.A. Santos, M.L. Moreira, D.P. Volanti, S.R. Teixeira, E. Longo, "Photoluminescence of barium–calcium titanates obtained by the microwave-assisted hydrothermal method (MAH)", *Chem. Phys. Lett.*, **488** [1-3] (2010) 54–56.
13. S. Jayanthi, T.R.N. Kutty, "Extended phase homogeneity and electrical properties of barium calcium titanate prepared by the wet chemical methods", *Mater. Sci. Eng. B*, **110** (2004) 202–212.
14. S.-S. Ryu, S.-K. Lee, D.-H. Yoon, "Synthesis of fine Ca-doped BaTiO_3 powders by solid-state reaction method – Part I: Mechanical activation of starting materials", *J. Electroceram.*, **18** (2007) 243–250.
15. X.N. Zhu, W. Zhang, X.M. Chen, "Enhanced dielectric and ferroelectric characteristics in Ca-modified BaTiO_3 ceramics", *AIP Advances*, **3** (2013) 082125.
16. A. Chaipanich, "Effect of PZT particle size on dielectric and piezoelectric properties of PZT-cement composites", *Curr. Appl. Phys.*, **7** (2007) 574–577.
17. G. Ye, J. Wade-Zhu, J. Zou, T. Zhang, T.W. Button, J. Binner, "Microstructures, piezoelectric properties and energy harvesting performance of undoped $(\text{K}_{0.5}\text{Na}_{0.5})\text{NbO}_3$ lead-free ceramics fabricated via two-step sintering", *J. Eur. Ceram. Soc.*, **40** [8] (2020) 2977–2988.
18. S.-J. Chae, T.-G. Lee, D.S. Kim, S.-W. Kim, E.-J. Kim, S.-M. Park, W.-S. Kang, S.J. Lee, C.-Y. Kang, S. Nahm, "Superior piezoelectric properties of lead-free thick-films and their application to alternative multilayer actuator", *J. Alloys Compd.*, **834** (2020) 155079.
19. S.-J. Jeong, M.-S. Ha, J.-S. Song, "Effect of geometry on properties of multilayer structure actuator", *Sens. Actuators A*, **116** (2004) 509–518.
20. B.-K. Koo, M. Saleema, D.-H. Lim, M.-S. Kim, I.-S. Kim, S.-J. Jeong, "Fabrication of borosilicate-glass-coated CuAg inner electrode for multilayer ceramic actuator", *Sens. Actuators A*, **277** (2018) 8–17.
21. S.-Y. Yoo, J.-Y. Ha, S.-J. Yoon, J.-W. Choi, "High-power properties of piezoelectric hard materials sintered at low temperature for multilayer ceramic actuators", *J. Eur. Ceram. Soc.*, **33** (2013) 1769–1778.
22. K. Feliksik, M. Adamczyk–Habrajaska, J. Makowska, J. A. Bartkowska, T. Pikula, R. Panek, O. Starczewska, "The impact of the final sintering temperature on the microstructure and dielectric properties of $\text{Ba}_{0.75}\text{Ca}_{0.25}\text{TiO}_3$ perovskite ceramics", *Materials*, **17** (2024) 5210.
23. M. H. Khedhri, N. Abdelmoula, H. Khemakhem, R. Douali, F. Dubois, "Structural, spectroscopic and dielectric properties of Ca-doped BaTiO_3 ", *Appl. Phys. A*, **125** (2019) 193.
24. S.N. Borkar, P. Aggarwal, V.K. Deshpande, "Effect of calcium substitution on structural, dielectric, ferroelectric, piezoelectric, and energy storage properties of BaTiO_3 ", *Curr. Appl. Phys.*, **39** (2022) 205–213.
25. R.K. Basumatary, K.K. Singha, S. Sen, B.N. Parida, M.D.

- Ganesh, D. Pamu, S.K. Srivastava, R. Brahma, “Effect of Co doped BCT on structural, microstructural, dielectric, and multiferroic properties”, *Ceram. Int.*, **50** (2024) 36306–36319.
26. A. Dhahri, A. Belkahla, J. Laifi, S. Gouadria, M. Elhadi, J. Dhahri, E. Dhahri, “Crystal structure and dielectric properties of the Ca/Y co-substituted BaTiO₃”, *Inorg. Chem. Commun.*, **141** (2022) 109570.
27. H.J. Hwang, K. Niihara, “Perovskite-type BaTiO₃ ceramics containing particulate SiC: Part II Microstructure and mechanical properties”, *J. Mater. Sci.*, **33** (1998) 549–558.
28. C.Y. Chen, W.H. Tuan, “Mechanical and dielectric properties of BaTiO₃/Ag composite”, *J. Mater. Sci. Lett.*, **18** (1999) 353–354.